Electron correlation in CaF_2 studied in threshold-excited soft-x-ray fluorescence

J-E. Rubensson, S. Eisebitt,* M. Nicodemus, T. Böske, and W. Eberhardt
Institut für Festkörperforschung des Forschungszentrums Jülich, Postfach 1913, D-52425 Jülich, Germany
(Received 29 April 1994)

Threshold-excited soft-x-ray-fluorescence spectroscopy has been used to study several selectively excited electronic configurations in CaF_2, enabling the determination of specific interaction energies. In the decay of the Ca $2p$ core excitons via core-to-core fluorescence, final states of the $3s^{-1}3d$ configuration are populated. Here the exchange interaction between the remaining $3s$ electron and the excited $3d$ electron was measured, as well as the Coulomb interaction between the core hole and the excited electron. Furthermore, the influence of crystal-field splitting on the $3s^{-1}3d$ states has been studied, and it was found that all of these three interaction energies are interrelated. Using the Ca core-to-core fluorescence data as fingerprints for the $2p$ excited states, we determine upper limits for the $2p_{1/2}^{-1}3d \rightarrow 2p_{3/2}^{-1}$ Coster-Kronig yields and for the $2p_{3/2}$ ionization threshold which in the absorption spectrum is masked by the $2p_{1/2}^{-1}3d$ resonances. Our data are in conflict with optical and photoemission data, a conflict which is resolved by assuming the existence of an excitonic $2p^{-1}ns$ state unidentifiable in the Ca L absorption spectrum. In the threshold-excited F K fluorescence spectra a satellite is assigned to the decay of core hole states with an additional valence vacancy, making it possible to discuss the p-p correlation energy in the valence band. Finally, the influence on the fluorine valence band of an excitonic screening electron localized in various states primarily localized on the neighboring Ca ions is determined.

I. INTRODUCTION

With the development of bright synchrotron-radiation sources it has become possible to study the excitation energy dependence of soft-x-ray-emission (SXE) spectra. A rich phenomenology is encountered in the sub-keV region, where the impact of spectator vacancies as well as spectator electrons on the valence-band emission have been studied.[1-3] Interpretations of resonant phenomena in terms of inelastic scattering (resonant Raman scattering) have also been put forward.[1,4]

In general it has been demonstrated that the energy dependence of SXE spectra is determined by the complex core-hole excitation-emission dynamics and in general the assignment of these spectral features has lead to a deeper understanding of the electronic structure. The complexity of the dynamics, however, often makes it difficult to draw quantitative conclusions. In this paper the technique is applied to CaF_2, a compound whose local closed-shell structure emphasizes some aspects of electron correlation in solids. In the spectra we identify several excited electronic states, where specific interaction energies can be readily determined. We here expand on earlier work,[5] where we demonstrated the advantage of increased interpretability of core-to-core fluorescence spectra as compared to valence-to-core spectra. The insight into the dynamics gained from these type of studies may help in the interpretation of the more complicated valence-to-core spectra. Moreover additional lifetime information can be obtained by analyzing the line shape of the fluorescence, which is difficult for valence-to-core transitions.

CaF_2 has been frequently studied because of its technical importance, mainly due to the ability to form high-quality interfaces with Si and GaAs. The Ca $2p \rightarrow 3d$ absorption spectrum,[6-8] as well as the F K absorption spectrum[9-11] have been measured and discussed and the electronic decay of the core excited states has been analyzed.[9,12] CaF_2 has also been studied in photoemission spectroscopy[13-16] and electronic-structure calculations[11,17-19] have been performed. The F K emission, excited with MeV helium ions has been studied earlier, with the interest focused on the double excitation satellites.[20,21] Here we present spectra with a resolution sufficient to discuss the valence-band density of states. To our knowledge no Ca L emission results, with the exception of our precursory study,[5] have been presented so far.

CaF_2 is an ionic compound where the valence electrons have almost solely F p character, i.e., locally at the fluorine sites one can describe the electronic structure in terms of F atoms with a $2p^6$ configuration. Band-structure calculations attribute a fractional charge in the valence band of less than 0.03 to Ca atoms.[17] The valence-band dispersion is thus mostly determined by the interaction between the fluorine electrons, and due to the small overlap between fluorine orbitals from different sites the valence band is very narrow ($\approx$2.3 eV). The electronic interactions at the F sites thus involve long-range effects, but the importance of electron correlation in the narrow p band can be debated. The Ca atoms can for many purposes be treated as Ca^{2+} ions ($2p^63s^23p^6$) in a ligand crystal field. The crystal field is especially important for excitations involving d orbitals. In the simple cubic symmetry the degeneracy between orbitals of e_g symmetry, directed in between the F atoms, and orbitals of t_{2g} symmetry, directed towards the F atoms, is lifted.

Threshold excited Ca core-to-core fluorescence from

CaF_2 can, under the present experimental conditions, be interpreted as a two-step process. In the first step an electron from the Ca $2p$ level is promoted to a previously empty $3d$ orbital, and in the second step a $3s$ electron fills the $2p$ hole.[5] In the final Ca $3s^{-1}3d$ states the Coulomb and exchange interaction between the $3s$ and the $3d$ electron can be directly measured. Tuning the excitation energy to different $2p^{-1}3d$ exciton states we can also determine the dependence of the crystal-field symmetry on the exchange and Coulomb interactions.

Threshold-excited core-to-core fluorescence constitutes a general method to study these interactions. The results are complementary to $3s$-level photoemission spectroscopy. For transition-metal compounds, the remaining $3s$ electron couples to incompletely filled d shells, giving rise to an exchange-split double structure.[22] The radiative deexcitation method introduces the additional aspect of a modification of the occupancy of the $3d$ shell, as we demonstrate below. Choosing $3d$ excitations of various symmetries is here instrumental for assigning the final states.

Using the SXE spectra as fingerprints for direct ionization we also discuss the energy of the $2p_{3/2}$ ionization threshold, and the probability for the $2p_{1/2}^{-1}3d \rightarrow 2p_{3/2}^{-1}$ Coster-Kronig (CK) decay of the $2p_{1/2}^{-1}3d$ excitation. We find evidence for an excitonic $2p_{3/2}^{-1}ns$ state masked in the absorption spectrum.

We also present the excitation energy dependence of the F K fluorescence spectrum. A SXE satellite is identified and assigned to transitions with a spectator valence-band vacancy. This allows us to draw conclusions about the correlation energies in the valence band. Comparing to spectra excited by helium ion impact we discuss the double excitation mechanism. We also measure the effect of an excitonic screening electron mainly localized on the neighboring Ca atoms, and find a difference in the interaction depending on whether this electron has predominately Ca s or d character.

II. EXPERIMENTAL

The experiment was carried out at the SGM monochromator at the X1B undulator beamline[23] at the NSLS in Brookhaven. The monochromatized beam from the moveable output slit was refocused onto the sample by means of a bendable float-glass mirror. The resolution of the incoming radiation was set to 0.6 eV. The fluorescence was analyzed in a recently constructed grazing incidence Rowland spectrometer.[24] It is equipped with four interchangeable spherical gratings to cover the spectral range from 30 eV to above 1 keV with high resolution and efficiency. The gratings and a position sensitive detector can be positioned and oriented along the various Rowland circles by means of computer controlled x-y and rotational tables. Input slit length and width, as well as the acceptance of the spectrometer can be varied *in situ* to match the efficiency and resolving power. To ensure that the Rowland focusing condition is fulfilled the optimum positions for the 0th and for the desired order of diffraction are determined, a procedure that is independent of possible small deviations from the specified grating parameters. The instrument uses holographic, ion-etched, gold-coated gratings, and the detector is based on a stack of multichannel plates and the resistive anode readout technique. To enhance the sensitivity in the grazing incidence geometry it is coated with CsI and an electron capturing electric field is applied at the surface. This procedure is proven to be of utmost importance for the sensitivity in a grazing incidence setup.[25]

For the Ca L core-to-core spectra we used a 30-μm input slit and a 5-m grating with 1200 lines/mm, giving a resolution of around 0.5 eV in the first order of diffraction. For the F K spectra a 10-μm input slit and the same grating as above were used in the second order of diffraction, giving a resolution of 0.4 eV. We combined the photoemission binding-energy values for the Ca $2p_{3/2}$, $2p_{1/2}$, and $3s$ electrons in CaF_2 (Ref. 13) set the energy scale of our Ca L emission spectrum excited above threshold. This gives the emission peak positions at 301.9 and 305.4 eV, and all the Ca L spectra are measured relative to those values with very high accuracy. The values are also used to refer the energy scale of the F K spectra, here the absolute error may be as large as 1 eV, even though the spectra are well referred relative to each other. For ionic compounds it is known that phonon relaxation effects may shift the SXE structures up to 1 eV relative to what is expected from photoemission.[26] Such effects would correspondingly uniformly shift all our measured structures. It would, however, not influence the discussion that is primarily focused on energy differences. The spectrometer will be described in detail elsewhere.[24]

The sample was a CaF_2 powder pressed into an indium foil. It is well-known that synchrotron radiation induces fluorine desorption [10] and it has been shown that electron-yield (EY) spectra exhibit changes after exposure to white light.[8] After 30-min exposure to the intense monochromatic light tuned to the strongest absorption peak in the Ca L spectrum we notice small changes in the EY spectra.[5] Even though these changes probably are insignificant for the much more bulk sensitive fluorescence measurement, we took care in always measuring on previously unexposed spots for less than 30 min at the sharp resonances. Somewhat longer (two or three times) exposure times were used off resonance.

III. RESULTS AND DISCUSSION

A. The Ca $2p \rightarrow 3d$ excitations

The Ca L EY absorption spectrum of CaF_2 shown in Fig. 1 (Ref. 6) has been successfully interpreted on the basis of model calculations for a Ca^{2+} ion in a ligand field, using parameters for spin-orbit coupling, p-d Coulomb and exchange interaction, and for the crystal-field splitting.[7,8] The calculations are performed in intermediate coupling, basically treating the core electrons in a jj coupling scheme due to the large spin-orbit interaction, and the outer electrons, for which the spin-orbit interaction is less important, in LS coupling.

Without crystal-field interaction one would expect three $2p^{-1}3d$ states in intermediate coupling: In the

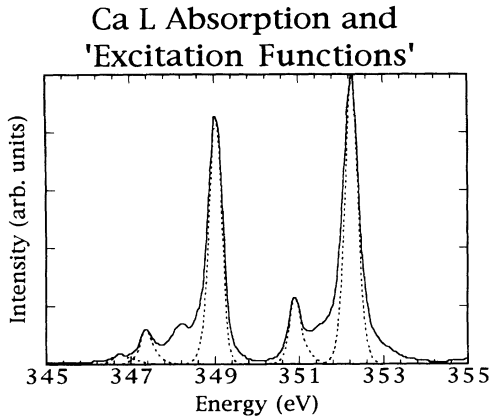

FIG. 1. Electron-yield absorption spectrum (Ref. 6) (solid line) and excitation functions (dashed lines) calculated by multiplying the spectrum with a normalized Gaussian of FWHM=0.6 eV.

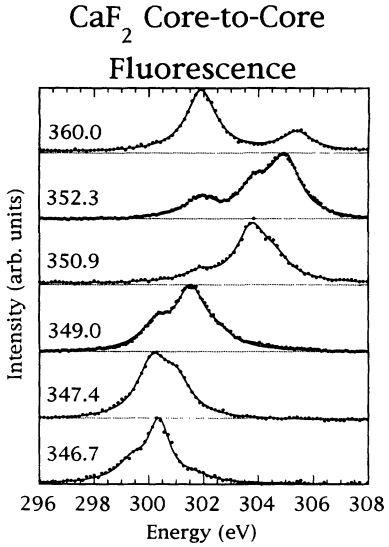

FIG. 2. Soft-x-ray-fluorescence spectra excited at the indicated energies (eV). The spectra should be associated with excitation functions in Fig. 1. The solid lines are the results of a curve fit as described in the text.

"near-LS limit" the dominating terms would be ^3P, ^3D, and ^1P, but the terms are mixed and the angular momentum cannot be unambiguously assigned to L and S. With the simple cubic crystal field the states are split into e_g and t_{2g} symmetry. The splitting can be directly related to the lifting of the degeneracy of the d orbitals, depending on their spatial orientation in between the fluorine atoms (e_g), or in the direction of the fluorine atoms (t_{2g}). A t_{2g} electron is thus subject to an antibonding interaction with the fluorine electrons whereas the e_g electron interacts only weakly with the surrounding. In summary, many types of interactions of the same order of magnitude result in a complex absorption spectrum, and at least seven peaks have been detected and assigned.

We adopt the following simplified view of the Ca L absorption spectrum. The two largest peaks at 349.0 and 352.3 eV we associate with the $2p_{3/2}^{-1}t_{2g}$ and the $2p_{1/2}^{-1}t_{2g}$ ($3d$ electron in t_{2g} symmetry) states, respectively. The two smaller peaks at 347.4 and 350.9 eV we associate with the $2p_{3/2}^{-1}e_g$ and $2p_{1/2}^{-1}e_g$ ($3d$ electron in e_g symmetry) states, respectively. Even though this simple picture is formally questionable, it is instrumental in the analysis of the decay spectra. The small peak at 346.7 eV, finally, we will call the ^3P peak since it primarily must be associated with that atomic term.[7]

Also included in Fig. 1 are the "excitation functions" which are simply a normalized Gaussian with a full width at half maximum (FWHM) of 0.6 eV (the monochromator function) multiplied with the absorption spectrum. These functions show the primary excitations that we monitor in the SXE spectra. We see in Fig. 1 that the resolution is sufficient to select the decay corresponding to every single absorption peak separately, with the exception of the ^3P state, where emission from the $2p_{3/2}^{-1}e_g$ state may contribute.

B. The Ca $3s \rightarrow 2p$ fluorescence

The SXE spectra corresponding to these excitation functions are shown in Fig. 2. We see a dramatic excitation energy dependence, where a change in the monochromator energy of less than 1 eV has a large impact on the spectral shape. We see SXE intensity move with the excitation energy as it is tuned over the absorption resonances, and far above threshold at 360 eV (top curve) the conventional fluorescence, corresponding to a $3s$ electron falling into the spin-orbit $2p$ ($\frac{3}{2},\frac{1}{2}$) hole, is detected. This is consistent with the general picture of soft-x-ray Raman scattering developing into fluorescence over resonances at core excitation thresholds,[27] which is the proper starting point for the analysis of this type of data. As shown above, however, in this case only intensity from one intermediate state is observed at each selected excitation energy. The energy separation between the electronic states is also large compared to their inherent lifetime width (<0.2 eV). Under these circumstances, with the excitation functions centered on the absorption peaks, the scattering picture and the conceptually simpler absorption followed by emission picture become equivalent. With an order of magnitude larger resolving power of the monochromator than in the present case coherent effects may become detectable. Here we will use the two-step picture and consider how final $3s^{-1}3d$ states are populated via the decay of the various $2p^{-1}3d$ intermediate states.

The moving SXE intensity is simply explained by the fact that intermediate states of various energies populate the same final states. This presumes that the excited electron is localized during the core-hole lifetime, which has already been demonstrated in the excitation energy dependence of the electronic decay.[9] We will show below that the excited electron stays during the SXE process as a spectator in the orbital of the primary excitation. We thus continue our interpretation within in the simple orbital scheme that we used for the $2p$ excitations. For Ca $3s$ hole states in the free atom case it has been shown that

a considerable configuration interaction occurs,[28,29] rendering the single-particle treatment questionable. In the present case, however, we show that the simple picture can be used to assign the structures in our spectra.

The solid lines in Fig. 2 are the result of a curve-fitting procedure. An initial Voigt curve fitting showed that in most cases the Lorentzian component is fully dominating, and we chose to use pure Lorentzians for simplicity. For many peaks the FWHM exhibits a value close to 1.3 eV, and with the present data quality no significant deterioration of the fit is introduced by locking the width of the Lorentz curves to this value. The exception is the narrow peak in the spectrum excited at 346.7 eV (Fig. 2, bottom) which has a Lorentz FWHM of 0.95 eV.

C. The Ca $3s^{-1}$ $3d$ final states

The contributions to the spectra from the various Lorentzian curves are shown in Fig. 3, and in Fig. 4 we plot the fitted peak positions as a function of the excitation energy. The solid lines in Fig. 4 describe the curves

$$E_s = E_p - E_f \ , \tag{1}$$

where E_s and E_p are the secondary energy (peak position), and the primary monochromator energy, respectively. The energy position of a peak corresponding to a transition into the same well-defined final state of energy E_f would follow this equation. At least three lines of this kind can be fitted, and splitting the center line in Fig. 4 into two components improves the agreement with the data points. We have chosen this splitting also for intensity reasons considered below. The four lines correspond to final states of energy $E_f = 46.4$, 47.2, 47.4, and 48.6 eV.

The two dashed lines in Fig. 4 mark the positions of the peaks in the spectrum excited above the ionization limit at 360 eV. At higher excitation energies the excited electron is decoupled from the system and thus the energy positions of these peaks are constant at 301.9 and 305.4 eV, independent of excitation energy. Here the normal L emission is turned on and, as described above, we have used these energy positions to calibrate the energy scale. Also at lower excitation energies, even down to 346.7 eV, we find peaks at 301.9 eV. This is due to the finite width of the monochromator function and the lifetime broadening of the $2p^{-1}$ state. Excitations by the second-order spectral component of the primary excitation may also contribute. Later we will use the intensity variation of the 301.9-eV peak to discuss the $2p$ ionization threshold.

In Fig. 5 we plot the experimental spectra (except the high-energy excited spectrum) on a "binding-energy scale" determined by the subtraction of the emission en-

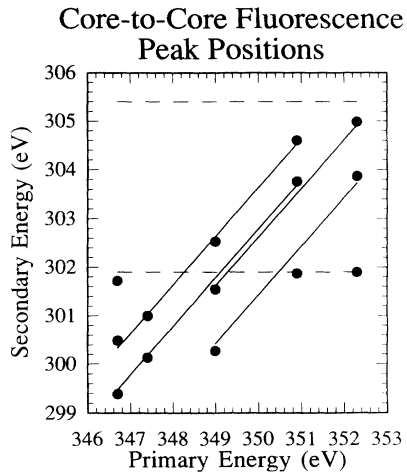

FIG. 4. Peak positions as a function of excitation energy. The four straight lines have the slope of unity, and correspond to excitations of 46.4, 47.2, 47.4, and 48.6 eV.

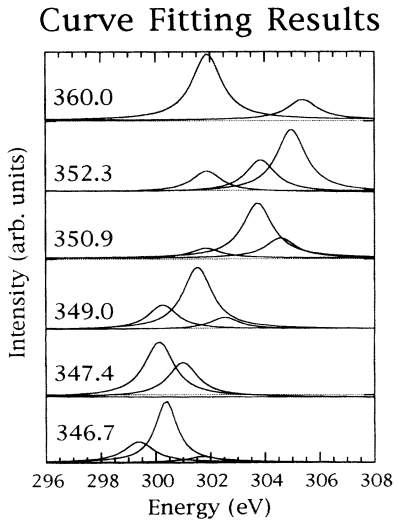

FIG. 3. The curve fit presented in Fig. 2, decomposed into its Lorentzian components. The FWHM is 1.3 eV except for the narrow peak in the spectrum excited at 346.7 eV, where the FWHM is 0.9 eV.

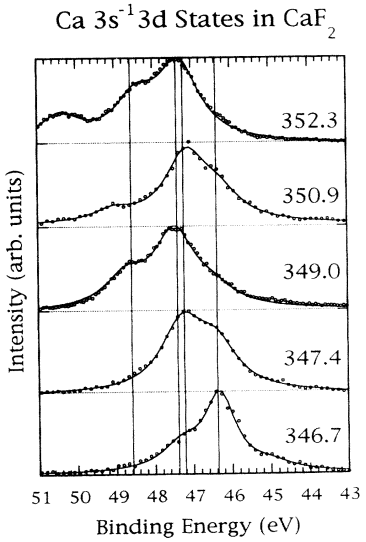

FIG. 5. The fluorescence spectra put on a binding-energy scale. The vertical lines mark the same values as found for the excitations in Fig. 4.

ergy from the primary energy. The E_f values determined above are marked with vertical lines, each corresponding to a specific final-state configuration.

We will now use the excitation energy dependence to assign the final states. We first use the fact that the state at $E_f=48.6$ eV has a significant intensity only at the excitation energy of 349.0 and 352.3 eV, i.e., where the intermediate states can be described as $2p_{3/2}^{-1}t_{2g}$ and $2p_{1/2}^{-1}t_{2g}$, respectively. During the decay the excited electron stays as a spectator in the t_{2g} orbital, and we believe that the probability for a shakedown process where the excited electron hops to an e_g orbital is small. The difference in spatial orientation of these orbitals supports this assumption. Hence, the state at $E_f=48.6$ eV is unambiguously of t_{2g} symmetry.

Using this argument we can also separate the states at $E_f=47.2$ and $E_f=47.4$ eV. At 349.0- and 352.3-eV excitation energy, where t_{2g} symmetry core excitons are excited, we find the peak maxima in Fig. 5 at higher binding energy than at 347.4- and 350.9-eV excitation energy. In the latter cases the intermediate states are $2p_{3/2}^{-1}e_g$ and $2p_{1/2}^{-1}e_g$, and the final states are accordingly of e_g symmetry. It immediately follows from Fig. 5 that the state at $E_f=47.4$ eV is of t_{2g} symmetry and that the state at $E_f=47.2$ eV is of e_g symmetry. Analogously we assign e_g symmetry to the state $E_f=46.4$ eV.

The splitting within the final $3s^{-1}3d$ states of the same symmetry is due to the $3s3d$ exchange splitting between the singlet and the triplet configuration. As we have shown earlier[5] the triplet states can be reached in dipole transitions from the singlet ground state, since S is undefined in the intermediate state. In the final states it is again legitimate to assign a defined spin to the states since the spin-orbit interaction is small. It is thus straightforward to construct the energy diagram of the Ca $3s^{-1}3d$ states in CaF_2 (see Fig. 6).

D. The 3s-3d exchange and Coulomb interaction in the crystal field

From Fig. 6 it is obvious that the exchange interaction is symmetry dependent. For states of e_g symmetry we find an exchange splitting of 0.85 eV, whereas for t_{2g} symmetry the splitting is 1.19 eV. We estimate the error to be less than 0.10 eV. The t_{2g} value is smaller, though within the error limits, than the value reported earlier,[5] due only to the different data analyses. The analysis is, in this case, based on the reasonable assumption that the curve shapes of the two components are identical, and it can thus be regarded as more reliable.

An atomic calculation for a free Ca^{2+} ion, based on the density-functional theory in the local-spin-density approximation,[30] including exchange and correlation from the homogeneous electron gas predicts the splitting to be 0.89 eV.[31]

We speculate that the splitting is larger in the t_{2g} case because of the antibonding overlap with the F orbitals. This tends to concentrate the charge of the excited electron more than in the free atom and in the e_g case, and consequently the exchange interaction with the $3s$ electron increases. The e_g orbital, being oriented in between the F atoms, retains its atomic properties to a larger extent, and the exchange splitting is in agreement with the calculated atomic value.

In Fig. 6 we also note that the crystal-field splitting is larger in the singlet case than in the triplet case, 1.36 and 1.02 eV, respectively. This is a direct consequence of the charge localization discussed above.

If we assume that the $2p^{-1}3d$ states are well described as two crystal-field split spin-orbit components we can also discuss the excitonic Coulomb interaction between the core holes and the excited electron. The difference in the $3d$ excitonic binding energy, comparing a $2p$ and a $3s$ hole, ΔC, is determined by comparing the transition energies in the neutral and the ionized systems as illustrated in Fig. 7. We assume that the exchange interaction splits the final states symmetrically according to the simple rule of adding and subtracting the exchange integral for the singlet and the triplet states, respectively. Thus, we can use the mean values of the transition energies associated with these states to determine E_n in Fig. 7. Using the peak values from the curve fit we get $\Delta C=0.9$ and $\Delta C=1.1$ eV for the $j=\frac{3}{2}$ and $j=\frac{1}{2}$ excitations of t_{2g}

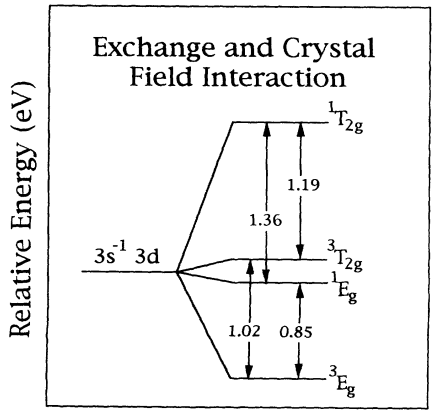

FIG. 6. The measured exchange and crystal-field splitting energies of the Ca $3s^{-1}3d$ electronic configuration of CaF_2, according to the assignment described in the text.

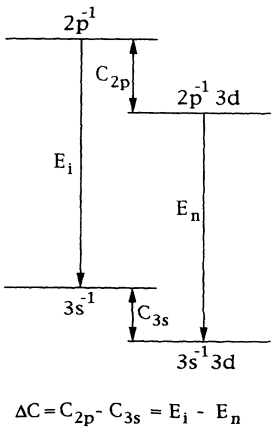

FIG. 7. The difference in $3d$ Coulomb screening comparing a $2p$ and a $3s$ core hole, ΔC, is measured by comparing the transition energies in the neutral and the ionized system, E_n and E_i.

symmetry, respectively, whereas for the e_g symmetry the value is $\Delta C = 1.3$ for both j values. Even though the first discrepancy is significant, the close agreement between the values for the same symmetry supports the initial assumption about the intermediate states. It is evident from these values that the $3d$ electron is more closely bound to a $2p$ hole than to a $3s$ hole, and that this difference is larger for the e_g than for the t_{2g} symmetry. The ΔC values have to be treated with caution since they are influenced by phonon relaxation if the ionized intermediate states relax more than the excitonic states before the SXE process occurs. This has been observed for other ionic compounds,[26] and we note that this effect would tend to decrease our ΔC values, since phonon relaxation after core ionization may be larger than after a charge preserving core excitation.

In Fig. 8 we see that the triplet-singlet intensity ratio is around 2.3, somewhat smaller than the statistical value of 3, for the t_{2g} symmetry, whereas it is much less, around 0.5, for the corresponding e_g excitations. For both symmetries the ratio decreases when going from the $2p_{3/2}^{-1}3d$ to the $2p_{1/2}^{-1}3d$ states. For the ^3P excitation the SXE spectrum is consistent with a statistical triplet-singlet intensity ratio of e_g symmetry. To understand the intensity variation of the peaks in detail a calculation is needed. We believe that a first step would be to use a parameter model of the type used to describe the absorption spectrum. Our data would then serve as a consistency check for the parameter set. This is beyond the scope of this paper.

Finally we note two spectral details that the above analysis does not account for. We do not understand why the main peak in the SXE spectrum excited at 346.7 eV has a FWHM of only 0.95 eV. The Lorentzian shapes indicate that lifetime broadening of the final states is the dominating broadening mechanism. The position of the peaks suggests that they are due to the ^3E_g and ^1E_g final states, in which case the FWHM for the strong peak should be larger. As seen in Fig. 1 the excitation function includes some of the $2p_{3/2}^{-1}e_g$ excitation. This inclusion could however not lead to a narrowing of the peak.

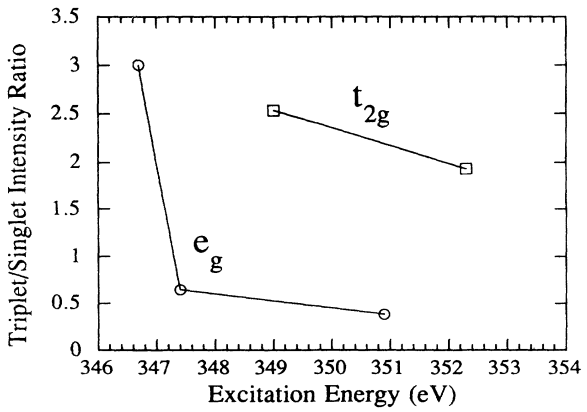

FIG. 8. The triplet-singlet intensity ratio for the two symmetries.

In the analysis of the spectrum excited at 349 eV we have to include a third peak to account for the width of the most intense structure. The peak fit puts this extra peak with around 15% of the full intensity at the position of the ^3E_g final state. This suggests that a shakedown of the d electron from the t_{2g} to the e_g orbital does occur.

E. The Ca $2p_{3/2}$ ionization threshold and the Coster-Kronig yield

In the SXE spectra excited at 350.9 and 352.3 eV there is a peak emerging at 301.9-eV energy. Since these peaks coincide with the 301.9-eV peak in the spectrum excited well above the ionization limit they obviously have to be assigned to the same $2p_{3/2}^{-1} \rightarrow 3s^{-1}$ transition. The appearance of this transition implies that the $2p_{3/2}$ ionization threshold is situated close to the $2p_{3/2}^{-1}3d$ resonances, and an analysis of the intensity variation with excitation energy should reveal the onset of the continuum transitions.

Also in the spectrum excited at the ^3P peak at 346.7 eV there is emission intensity at 301.9 eV. This peak has to be attributed to the transition in the ionized system. First of all, since the absorption probability is small at this energy, there is a finite contribution from the tail of the monochromator function. In this case, however, we can also attribute the observation of this transition to excitation processes due to the second order of the primary radiation. The intensity is so small that the corresponding transition from the spin-orbit partner at 305.4 eV would be unmeasurable with our present sensitivity. This puts an upper limit to contributions from the second order, and we conclude that such contributions can be ruled out at the other excitation energies.

We will now use the excitation energy dependence of the emission spectra to determine the position of $2p_{3/2}$ ionization threshold, and estimate the ionization cross section. This cannot be done directly in the absorption spectrum since the $2p \rightarrow 3d$ transitions fully dominate at these excitation energies. Furthermore, we will discuss the importance of the $2p_{1/2}^{-1}3d \rightarrow 2p_{3/2}^{-1}$ Coster-Kronig decay.

If the self-absorption of the outgoing photons is neglected, and the two-step model for the emission-absorption process is assumed, the fluorescence intensity ratio I_i/I_n associated with transitions in the ionized and the neutral system can be written

$$\frac{I_i}{I_n} = \frac{P_i\omega_i + P_n\omega_{CK}\omega_i}{P_n(1-\omega_{CK})\omega_n} , \tag{2}$$

where P_i and P_n are the excitation probabilities for the ionized and neutral intermediate states, respectively. The neutral $2p_{1/2}^{-1}3d$ states may decay to the ionic $2p_{3/2}^{-1}$ state with the Coster-Kronig yield ω_{CK}. ω_i is the $2p^{-1} \rightarrow 3s^{-1}$ fluorescence yield, and ω_n is the $2p^{-1}3d \rightarrow 3s^{-1}3d$ yield in the case where $\omega_{CK}=0$. Under the reasonable assumption that $\omega_i = \omega_n$ one arrives at the following simple relation:

$$P_i = P_n \left[\frac{I_i}{I_n} - \omega_{CK} \left[\frac{I_i}{I_n} + 1 \right] \right] . \quad (3)$$

For the excitation probabilities we have

$$P_k = \int A_k(E) M(E) dE , \quad (4)$$

where $k = i$ and $k = n$ for the ionization and the excitation processes, respectively. $A_k(E)$ is the absorption cross section associated with the process in question and $M(E)$ is the monochromator function. The latter is a Gaussian with a FWHM of 0.6 eV. For the neutral excitations we assume that $A_n(E)$ is proportional to the absorption spectrum itself, since the neutral excitations are dominating. We determine P_n according to Eq. (4) using the absorption spectrum of Fig. 1, normalized to unity at the maximum. The intensity ratio, I_i/I_n, is readily measured for the fitted curves, using the assignment above. Through Eq. (3) we now know the relation between the direct ionization probability and the probability for ionization via the Coster-Kronig process. We first look at the limiting case where ω_{CK} is zero.

Then $P_i(E)$ can be unambiguously determined, and we show the results in Table I and in Fig. 9. The solid curves in Fig. 9 are $P_i(E)$ determined according to Eq. (4), where we have assumed a step function convoluted with a Lorentzian of 0.2-eV FWHM for $A_i(E)$. We use the step height and edge position of $A_i(E)$ to fit the measured data. We thus determine the ionization threshold at 351.3 eV and the ionization step height to amount to about 13% of the most intense peak in the absorption spectrum.

We note that the analysis is consistent with the fact that we do not detect any peak at 301.9 eV in the spectra excited at 347.4 and 349.0 eV. From Fig. 9 we estimate that the I_i/I_n in these cases would be 0.027 and 0.008 which is below our detection limit.

The intensity measured at 301.9 eV measured in the spectrum excited at the ^3P peak is about a factor of 2 larger than we expect from the edge analysis. The ionization probability is here around than 0.1% of the main peak excitation probability. A contribution from the second order of the monochromator explains the discrepancy.

An ionization edge at 351.3 eV which a step height of 13% of the strongest absorption feature is not consistent with the absorption spectrum. In Fig. 9(b) we plot our calculated edges together with the absorption spectrum,

TABLE I. The measured intensity ratio I_i/I_n between intensity assigned to transitions in ionized (I_i) and neutral (I_n) CaF_2. The probability for neutral excitations (P_n) is determined from Eq. (4), i.e., integrating the excitation functions in Fig. 1. The probability for direct ionizations (P_n) according to Eq. (3) assuming that $\omega_{CK}=0$.

Energy (eV)	I_i/I_n	P_n	P_i
346.7	0.069	0.020	0.0014
350.9	0.13	0.14	0.018
352.3	0.22	0.59	0.13

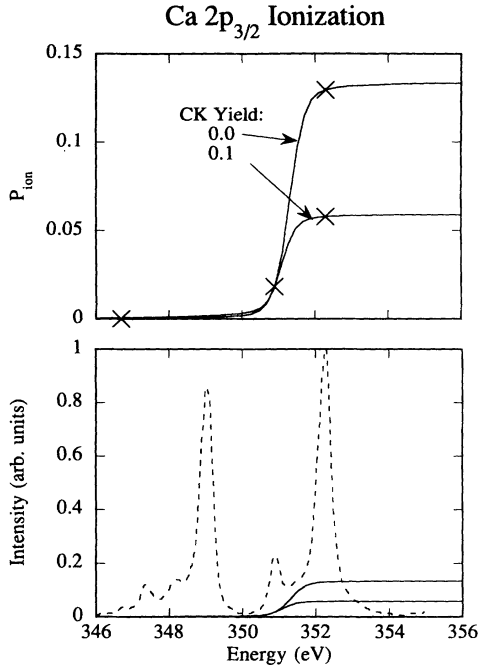

FIG. 9. The energy dependence of the probability for direct $2p_{3/2}$ ionization. A step function broadened with a Lorentzian with a width of 0.2 eV is used for the onset of ionization. If the Coster-Kronig yield is neglected the two high-energy points a threshold at 351.3 eV and a step-height of 13% of the intensity maximum in the absorption spectrum are derived. With increasing CK yield the step height and the threshold values decrease. For the small step height a CK yield of 0.10 is assumed for the $2p_{1/2}^{-1}t_{2g}$ state. The data are shown in Table I.

which is obviously lacking a step at the corresponding energy.

The $2p_{3/2}$ ionization can, however, occur indirectly. The most intense $2p_{1/2}^{-1}3d$ excitation is found above the $2p_{3/2}$ ionization limit, leaving the $2p_{1/2}^{-1}3d \rightarrow 2p_{3/2}^{-1}$ Coster-Kronig decay channel open. A finite CK yield would result in fluorescence from ionized states, and hence decrease the estimated continuum edge height, as is expressed in Eq. (3). We show the edge behavior in Fig. 9(a) when $\omega_{CK}=0.0$ an 0.1. In the limiting case where the probability for direct ionization is negligible we can determine the upper limit for the CK yield according to Eq. (3) and the measured intensity ratios in the SXE spectra. We get $\omega_{CK}^{max}=0.18$ for the $2p_{1/2}^{-1}t_{2g}$ state and $\omega_{CK}^{max}=0.12$ for the $2p_{1/2}^{-1}e_g$ state. This would however put the ionization limit at energies much lower than 351.3 eV which is unreasonable since the excitonic nature of the 349.0-eV excitation has been clearly demonstrated. Thus, we conclude that the first limit ($\omega_{CK}=0$ for t_{2g} and ionization limit 351.3 eV) is incompatible with the absorption spectrum, and that the second limit ($\omega_{CK}=0.18$ for t_{2g} and ionization limit much lower than 351.3 eV) can be ruled out for energy reasons.

In fact even the upper limit, 351.3 eV, for the ionization energy is too low to be consistent with other experimental results. Using the literature value for the optical

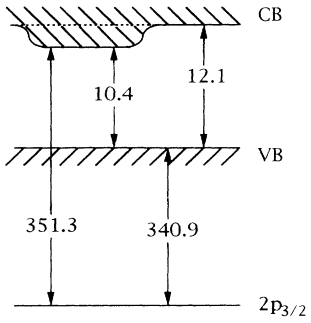

FIG. 10. Electronic level scheme demonstrating the incompatibility of our observation with photoemission (Ref. 10) and reflectivity (Ref. 18) data. This discrepancy can be resolved by the existence of weakly bound excitonic Ca $2p^{-1}ns$ states.

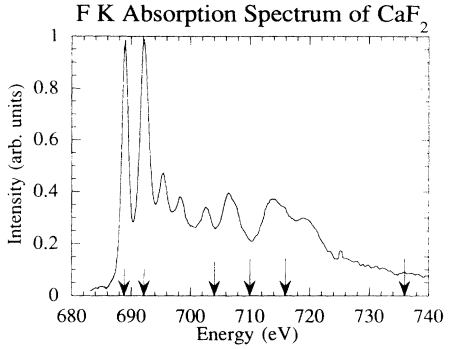

FIG. 11. The F *K* absorption spectrum (Refs. 10 and 23) with the excitation energies for the fluorescence spectra indicated.

band gap [12.1 eV (Ref. 18)] and photoemission data for the binding-energy difference of the valence-band edge and the $2p_{3/2}$ level [340.9 eV (Ref. 9)], we find the $2p_{3/2}$ conduction-band-edge energy separation at 353 eV. This is clearly in conflict with our measurement, as is illustrated in Fig. 10.

We propose a way to resolve these discrepancies by assuming that excitonic *s*-like states are pulled down into the gap in the presence of the core hole. An electron in such a state, acting as a spectator during the SXE process would probably not influence the spectral shape, due to the limited interaction with the core. The lack of dispersion would indicate that the excitonic binding energies are identical in the initial and final states, i.e., the Coulomb attraction energy would be the same for a $2p^{-1}ns$ and a $3s^{-1}ns$ exciton.

F. F $2p \rightarrow 1s$ fluorescence

For materials where correlation is less important SXE spectra associated with an electron from the valence band filling a core hole can be taken as a measure of the local density of occupied states (LPDOS). The locality comes from the localization of the initial core hole, and "partial" refers to the dipole selection rule that allows valence states only of certain angular momentum symmetry. In this noncorrelated limit the F *K* emission spectrum would map the *p*-projected valence DOS, locally around the fluorine atoms. As mentioned in the introduction, the valence band in CaF_2 is overwhelmingly of F $2p$ character, and we expect, within this picture, a similar spectral shape as measured in direct photoemission. A possible difference is due to a difference in the energy dependence of the matrix elements, which we find unlikely over the small valence bandwidth. Differences can also be due to the different initial states. In photoemission the final states are reached from direct ionization of the ground state, whereas in SXE they are reached in a charge-conserving process from the core hole state. Phonon broadening mechanisms would contribute differently for the two processes.

Also in the case of the F *K* fluorescence spectra we find a dramatic excitation energy dependence. In Fig. 11 we show the EY absorption spectrum,[10,23] and indicate with arrows the excitation energies used to record the SXE spectra. When the excitation energy is tuned close to the excitation threshold the width of emission profile is changing as can be seen in Fig. 12. At an excitation energy of 688.9 eV, corresponding to the first sharp peak in the absorption spectrum we measure a FWHM of 1.45 eV, and at 692.3 eV, the position of the second peak in the absorption spectrum, the FWHM has increased to 1.9 eV. It turns out that the value increases to 2.2 eV at higher excitation energies (700–740 eV) as can be seen in Figs. 13 and 14. At these energies the shape of the main peak is constant within the present measurement accuracy. Furthermore a satellite peak develops at around 679-eV emission energy. The satellite is first seen at 710-eV excitation energy and the intensity relative to the main line increases to around 13% at 736-eV excitation energy. The situation is illustrated in Fig. 14.

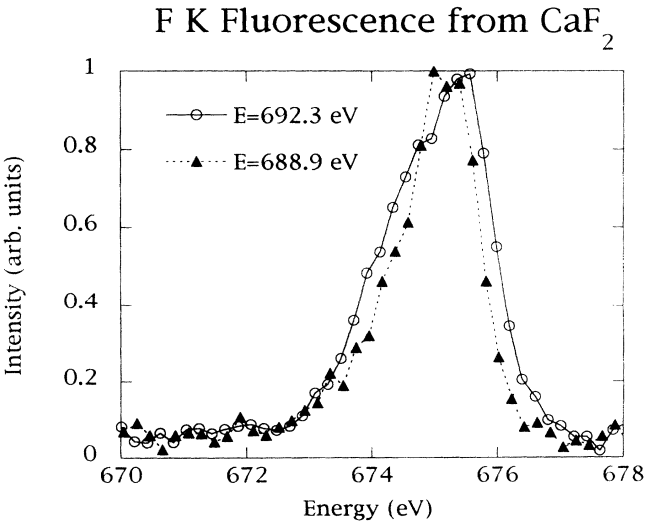

FIG. 12. F *K* fluorescence spectra excited on the first two absorption peaks.

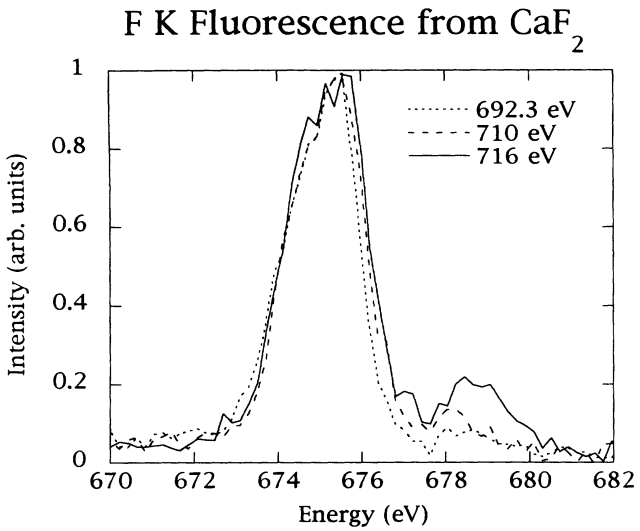

FIG. 13. F K fluorescence spectra at higher excitation energies, showing the onset of the satellite.

G. The spectator vacancy satellite

The appearance of the satellite is already indicative of correlation. As can be seen in Fig. 14 the satellite intensity increases dramatically for excitation energies above 715 eV. The intensity behavior is thresholdlike and nonresonant. Thus, the satellite intensity variation is indicative of intermediate states populated in shake processes. For energy reasons we can discard the possibility that the intensity originates from recombination of excitonic states. It has been shown that such states, populated via shake processes give rise to SXE satellites in boron compounds.[3] We assign the satellite to transitions where an additional vacancy in the valence band has been created in the initial excitation process. This vacancy stays as a spectator during the subsequent SXE decay and shifts the transition energy. This type of satellite is frequently seen, e.g., in high-energy excited L emission spectra of transition metals and their compounds,[1,32] where extra vacancies in the localized d orbitals cannot be screened during the core hole lifetime. Analogously, we find that the F 1s core hole lifetime is shorter than the time scale for the screening processes in the narrow 2p valence band. Double vacancy satellites in ionic compounds have been discussed in connection with spectra excited by high-energy helium ions.[20,21] Satellite to main line intensity ratios are much higher with this means of excitation, and with 2-MeV ion impact the F K satellite intensity in CaF_2 is even larger than the main line intensity.[20] At our highest excitation energy (736 eV) we are roughly 20 eV above the double ionization threshold, and it is likely that the intensity ratio increases by around a factor of 2 or 3 towards the sudden limit.[32,33] It is not possible, however, to reach the intensity ratio values found by ion impact. This leads to the conclusion that the excitation mechanism in the He ion bombardment case cannot solely be shakeoff processes.

With this assignment it is straightforward to measure the correlation energies. From the energy scheme in Fig. 15 it can be deduced that the binding energy of a 2p electron is 3.2 eV larger in the $1s^{-1}$ than in the $2p^{-1}$ configuration. This value is just the satellite-to-main line energy shift which is independent of the absolute energy calibration. As illustrated in Fig. 15 it can be directly related to the difference between the 1s-2p and the 2p-2p Coulomb repulsion energies, U_{1s2p} and U_{2p2p}. The value of 3.2 eV is comparable to the corresponding values for gas-phase Ne,[34] where three transitions from the triplet and singlet $1s^{-1}2p^{-1}$ states are spread out from 3.4 to

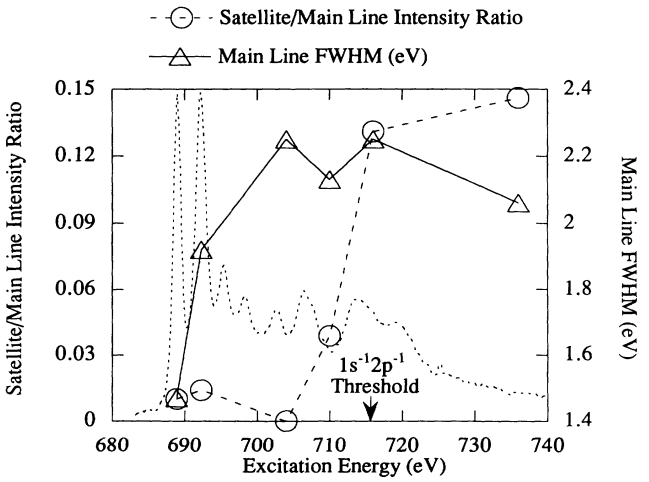

FIG. 14. Excitation energy dependence of the FWHM of the main structure, and of the satellite and main line intensity ratio. The latter is determined by integrate intensity in the regions 672–677.5 eV (main line) and 677.5–680.5 eV, after subtracting a quadratic background.

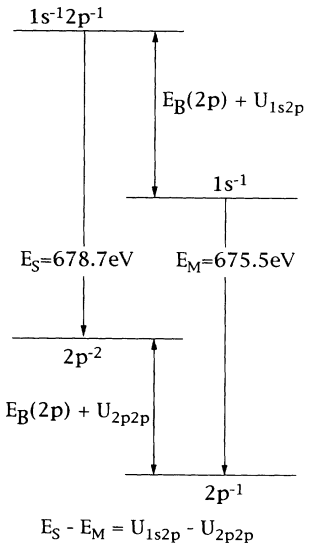

FIG. 15. Energy scheme for the fluorine excitations. The energy shift between the main line and the satellite determines the difference in Coulomb repulsion between a 1s and a 2p hole, U_{1s2p} and between two 2p holes, U_{2p2p}.

7.1 eV above the main line. Smaller shifts and smaller variations due to atomiclike coupling are found for free molecules of first-row elements.[35,36] It has been shown, in the case of H_2O, that it is important to consider the relaxation of the initial and the final states to get a realistic estimate of U_{1s2p} and U_{2p2p}. In that case reasonable prediction of the experimental results could be achieved within the Hartree-Fock approximation, also when discarding the relaxation due to the spectator vacancy.[36] The present results suggest that the situation in the narrow F $2p$ band of CaF_2 is similar to the free molecule case.

The satellite to main line intensity ratio is also much smaller compared to what is seen in high-energy-excited SXE spectra from comparable first-row molecules. The reason for the small satellite intensity as compared to free molecules could be that the shake probability is smaller, due to smaller intermediate state relaxation. One must also consider the hopping rate of the valence vacancy that may be comparable to the core hole decay rate. Unfortunately these two mechanisms cannot be distinguished in our experiment.

The $1s^{-1}2p^5$ threshold indicated in Fig. 14 has been calculated using the fact that the $1s^{-1}\rightarrow 2p^{-2}$ Auger process has the initial and the final state in common with the main line and the satellite SXE processes, respectively. The value of 715.7 eV is achieved by subtracting the value for the main line Auger, 649.5 eV,[13] from the sum of E_s, E_M and the F $2p$ binding energy, 11.0 eV.[14] In Fig. 14 it is clear that the satellite intensity threshold is displaced to lower energies relative to the double ionization threshold. This is not a contradiction since the first shakeup states must be of excitonic nature. The observation strongly suggests an interpretation of the absorption structure at 715 eV as due to $1s$ holes with additional excitonic interband excitations, a possibility that was ruled out by Gao *et al.*[11] for intensity reasons. In Ref. 11 a plasmon excitation is suggested as explanation for the absorption structure. Such a mechanism would probably not leave any fingerprint in the SXE spectra.

H. A screening electron on the neighbor atoms

We now turn our attention to the narrowing of the SXE main line as the excitation energy is tuned to the two first structures in the absorption spectrum. The excitonic origin of the sharp features has been demonstrated theoretically,[11] and the electronic decay spectrum of states excited at the first peak[9] shows unambiguously excitonic behavior. The conduction-band states are to a large extent localized on the Ca ions, and have very little F p character. It has been proposed[9] that the first peak is to be associated with the lowest part of the conduction band, being mainly Ca $4s$, pulled down in the presence of the F $1s$ hole. The second peak corresponds to the Ca t_{2g} orbitals that to some extent can mix with the F p orbitals.[17] Following this interpretation we are faced with electrons that are screening the F $1s$ hole by being localized mainly on the nearest-neighbor Ca atoms. We believe that the SXE main band narrowing also can be understood in this picture.

The width of the valence band is determined by the bonding and antibonding overlaps of the F $2p$ orbitals, resulting in the largest bandwidth at the X point (slightly larger than at the Γ point) in the Brillouin zone,[17] whereas at the L points the band is much narrower. It is reasonable to assume that a screening electron on the neighboring Ca ions, would be compensated mainly via the bonding and antibonding states. It would tend to suppress the intensity in the spectra corresponding to these states, as seen in the SXE spectra excited on the first two excitonic absorption peaks. Thus, in those spectra the DOS peaks associated with the nonbonding orbitals are emphasized relative to the states with larger F-F overlap.

This is in agreement with the observation that the band narrowing is larger when the excited electron is in a Ca s-derived state (excitation on the first peak) than when it goes into a state of predominantly Ca d character. The difference in the valence-band linewidth originates in this simple picture from the difference in polarizability of the Ca orbitals.

I. The F 2p valence band

In Fig. 14 we see that for excitation energies in the region around 705 eV, where no screening narrowing is present and the satellite is turned off, we expect to get the best correspondence to the valence-band DOS and photoemission. In Fig. 16 we compare the spectrum excited at 710 eV, on a binding-energy scale, determined by subtracting the binding energy of the F $1s$ electron, 687 eV,[13] to the valence-band photoelectron spectrum from Ref. 16, energy shifted for comparison. The overall line shape is similar, even though the SXE spectrum is somewhat narrower. We note however, that the shape of the photoemission line is dependent on photon energy, as well as other experimental parameters such as the choice of substrate and sample preparation methods. The small hump at lower energies in the SXE spectrum is due to the onset of the satellite.

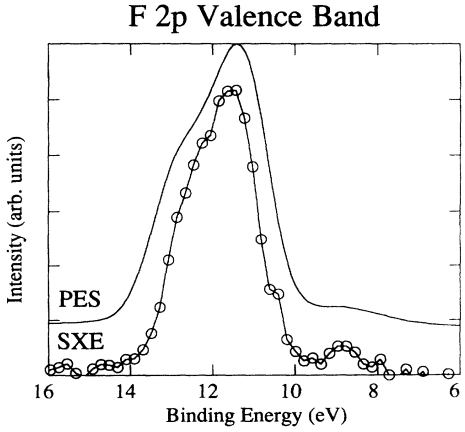

FIG. 16. The valence-band spectrum, excited at 710 eV put on a binding-energy scale and compared to the direct photoemission spectrum (Ref. 16).

IV. CONCLUSIONS

Threshold-excited SXE spectroscopy provides new insights about the electronic structure and excitation dynamics in CaF_2. Several electronic states have been identified, allowing us to determine various interaction energies. The magnitudes of the $3s$-$3d$ exchange and Coulomb interactions were determined in the Ca $3s^{-1}3d$ states, and it was shown how these interactions vary with the crystal-field symmetry. Also the crystal-field splitting of the states could be determined, and its dependence on the multiplicity was demonstrated. Regarding the band gap, our results are in conflict with photoemission and optical data. This discrepancy can be removed by assuming the existence of an excitonic Ca $2p^{-1}ns$ state. The F $1s^{-1}2p^{-1}$ satellite was identified and used to interpret structures in the F K absorption spectrum, and used to examine correlation energies in the valence band. The influence on the F $2p$ band of an excitonic screening electron on the neighboring Ca atoms was determined.

Core-to-core fluorescence demonstrates a promising application of threshold-excited SXE spectroscopy. In the case of correlated materials, the excitation-emission process can be used to reach and to characterize numerous hitherto unstudied electronic states. In the near future we intend to extend the core-to-core fluorescence studies to other ionic compounds.

ACKNOWLEDGMENTS

National Synchtrotron Light Source in Brookhaven is supported by the DOE, Offices of Basic Sciences. One of us (S.E.) is thankful for the support by the DAAD (HSPII). We are grateful for the technical assistance of J. Lauer, H. Feilbach, and D. Hoffman, for valuable discussions with K. M. Colbow, and for the help of B. Itchakwitz and P. D. Johnson at the X1B beamline.

*Also at Department of Physics, University of British Columbia, Vancouver, British Columbia, Canada V6T 1Z1.

[1]N. Wassdahl, P. Bleckert, G. Bray, P. Glans, N. Mårtensson, J. Nordgren, J-E. Rubensson, R. Nyholm, and S. Cramm, in *15th International Conference on X-ray and Inner-Shell Processes, Knoxville, TN,* AIP Conf. Proc. No. 215 (AIP, New York, 1990), p. 451, and references therein.

[2]J. J. Jia, W. L. O'Brien, T. A. Callcott, Q.-Y. Dong, J-E. Rubensson, D. R. Mueller, D. L. Ederer, Z. Tan, F. Namavay, and J. I. Budnick, Phys. Rev. Lett. **67**, 731 (1991).

[3]W. L. O'Brien, J. J. Jia, Q-Y. Dong, T. A. Callcott, K. E. Miyano, D. L. Ederer, D. R. Mueller, and C.-C. Kao, Phys. Rev. Lett. **70**, 238 (1993).

[4]Y. Ma, N. Wassdahl, P. Skytt, J. Guo, J. Nordgren, J.-E. Rubensson, T. Böske, W. Eberhardt, and S. D. Kevan, Phys. Rev. Lett. **69**, 2598 (1992).

[5]J.-E. Rubensson, S. Eisebitt, M. Nicodemus, T. Böske, and W. Eberhardt, Phys. Rev. B **49**, 1507 (1994).

[6]C. T. Chen and F. Sette, Phys. Rev. Lett. **60**, 168 (1988).

[7]F. M. F. de Groot, J. C. Fuggle, B. T. Thole, and G. A. Sawatzky, Phys. Rev. B **41**, 928 (1990).

[8]F. J. Himpsel, U. O. Karlsson, A. B. McLean, L. J. Terminello, F. M. F. de Groot, M. Abbate, J. C. Fuggle, J. A. Yarmoff, B. T. Thole, and G. A. Sawatzky, Phys. Rev. B **43**, 6899 (1991).

[9]T. Tiedje, K. M. Colbow, D. Rogers, and W. Eberhardt, Phys. Rev. Lett. **65**, 1243 (1990).

[10]W. Eberhardt, K. M. Colbow, Y. Gao, D. Rogers, and T. Tiedje, Phys. Rev. B **46**, 12 388 (1992).

[11]Y. Gao, T. Tiedje, P. C. Wong, and K. A. R. Mitchell, Phys. Rev. B **48**, 15 578 (1993).

[12]M. Elango, A. Ausmees, A. Kikas, E. Nõmmiste, R. Ruus, S. Saar, J. F. van Acker, J. N. Andersen, R. Nyholm, and I. Martinson, Phys. Rev. B **47**, 11 736 (1993).

[13]D. Rieger, F. J. Himpsel, U. O. Karlsson, F. R. McFeely, J. F. Morar, and J. A. Yarmoff, Phys. Rev. B **34**, 7295 (1986).

[14]M. A. Olmstead, R. I. G. Uhrberg, R. D. Bringans, and R. Z. Bachrach, Phys. Rev. B **35**, 7526 (1987).

[15]D. Mao, K. Young, A. Kahn, R. Zanoni, J. McKinley, and G. Margaritondo, Phys. Rev. B **39**, 12 735 (1989).

[16]K. M. Colbow, T. Tiedje, D. Rogers, and W. Eberhardt, Phys. Rev. B **43**, 9672 (1991).

[17]R. A. Heaton and C. C. Lin, Phys. Rev. B **22**, 3629 (1980).

[18]G. W. Rubloff, Phys. Rev. B **5**, 662 (1972).

[19]J. P. Albert, C. Jouanin, and C. Gout, Phys. Rev. B **16**, 925 (1977).

[20]G. Deconninck and S. van den Broek, J. Phys. C **13**, 3329 (1980).

[21]O. Benka, R. L. Watson, and R. A. Kenefick, Phys. Rev. Lett. **47**, 1202 (1981).

[22]C. S. Fadley, in *Electron Spectroscopy: Theory Techniques and Applications,* edited by C. R. Brundle and A. D. Baker (Academic, New York, 1978), Vol. 2, and references therein.

[23]K. J. Randall, J. Feldhaus, W. Erlebach, A. M. Bradshaw, W. Eberhardt, Z. Xu, Y. Ma, and P. D. Johnson, Rev. Sci. Instrum. **63**, 1367 (1992).

[24]J.-E. Rubensson, H. Feilbach, T. Böske, S. Eisebitt, J. Lauer, and W. Eberhardt (unpublished).

[25]J. Nordgren, G. Bray, S. Cramm, R. Nyholm, J-E. Rubensson, and N. Wassdahl, Rev. Sci. Instrum. **60**, 1690 (1989).

[26]W. L. O'Brien, J. J. Jia, Q-Y. Dong, T. A. Callcott, D. R. Mueller, and D. L. Ederer, Phys. Rev. B **45**, 3882 (1992).

[27]J. Tullki and T. Åberg, in *Atomic and Inner Shell Physics,* edited by B. Crasemann (Plenum, New York, 1985), and references therein.

[28]O. Walter and J. Schirmer, J. Phys. B **14**, 3805 (1981).

[29]J. M. Bizau, P. Gérard, F. J. Wuilleumier, and G. Wendin, Phys. Rev. A **36**, 1220 (1987).

[30]S. H. Vosko, L. Wilk, and N. Nussair, Can. J. Phys. **58**, 1200 (1980).

[31]B. Engels and S. Blügel (private communication).

[32]N. Wassdahl, J-E. Rubensson, G. Bray, P. Glans, P. Bleckert, R. Nyholm, S. Cramm, N. Mårtensson, and J. Nordgren, Phys. Rev. Lett. **64**, 2807 (1990).

[33]G. B. Armen, T. Åberg, Kh. R. Karim, J. C. Levin, B. Crasemann, G. S. Brown, M. H. Chen, and G. E. Ice, Phys. Rev. Lett. **54**, 182 (1985).

[34]H. Ågren, J. Nordgren, L. Selander, C. Nordling, and K. Siegbahn, J. Electron Spectrosc. **14**, 27 (1978).

[35]J-E. Rubensson, L. Pettersson, N. Wassdahl, M. Bäckström, J. Nordgren, O. M. Kvalheim, and R. Manne, J. Chem. Phys. **82**, 4486 (1985).

[36]J-E. Rubensson, H. Ågren, and R. Manne, J. Electron. Spectrosc. **36**, 307 (1985).